OPERATING EXPERIENCE WITH SUPERCONDUCTING RF AT CESR AND OVERVIEW OF OTHER SRF RELATED ACTIVITIES AT CORNELL UNIVERSITY[*]

S. Belomestnykh[+], P. Barnes, E. Chojnacki, R. Ehrlich, R. Geng[#], D. Hartill, R. Kaplan,
J. Knobloch, H. Padamsee, S. Peck, P. Quigley, J. Reilly, D. Rubin, D. Sabol, J. Sears,
V. Veshcherevich, G. Werner,

Laboratory of Nuclear Studies, Cornell University, Ithaca, NY 14853, U.S.A.

Abstract

In the two years past since 8th RFSC Workshop the major efforts of the SRF group at Cornell University were concentrated on the completion and commissioning of the superconducting RF system for the Cornell Electron Storage Ring (CESR) $e+e-$ collider [1, 2]. Four single-cell niobium higher-order mode (HOM) damped cavities replaced four 5-cell normal conducting RF cavities. The RF system upgrade began in 1997 and proceeded replacing cavity by cavity until installation of final SRF cavity in September 1999. Superconducting cavities helped CESR to reach total beam current of 550 mA in two beams and peak luminosity of 8.3×10^{32} cm^{-2}s^{-1}. The maximum power delivered to the beam via a ceramic vacuum RF window is 260 kW. The maximum HOM power absorbed by the ferrite HOM loads is 5.7 kW per cavity. The commissioning results and operating experience are discussed. During the same time period Cornell has continued basic SRF studies of cavity performance limitations and development of new techniques and tools for experiments, data analysis and computer simulations.

1 INTRODUCTION

The Cornell Electron Storage Ring (CESR) is a single-ring symmetric $e+e-$ collider operating on and near the Y(4S) resonance ($E \approx 5.3$ GeV). The beams collide with a small horizontal crossing angle (± 2.1 mrad) at a single interaction point where the CLEO detector is located. Also, CESR provides beams for experiments with synchrotron radiation at the Cornell High-Energy Synchrotron Source (CHESS). CESR has achieved a peak luminosity of 8.3×10^{32} cm^{-2}s^{-1}, a total beam current of 550 mA and a beam-beam tune shift parameter $\xi_v =$ 0.05. At present each beam consists of 36 bunches arranged in 9 bunch trains, each is populated with 4 bunches spaced by 14 ns.

CESR is nearing completion of a Phase III of its luminosity upgrade [3, 4] which includes upgrading its RF system from four 5-cell normal conducting cavities to four single-cell superconducting niobium cavities. This, together with installation of new interaction region (IR) optics in 2000, will lead to the total current increase up to 1 ampere and luminosity up to 2.0×10^{33} cm^{-2}s^{-1}. SRF cavities were chosen for the RF system upgrade because they are very well suited for high beam intensity by their inherently high fundamental mode shunt impedance and consequent high accelerating gradient, low R/Q of fundamental and higher-order modes, ease of thorough HOM damping and therefore low beam impedance and loss factor [5]. The high-gradient capability of the SRF system will allow a reduction in bunch length from 19 mm to 13 mm. The SRF system will support 1 A beam current by delivering 325 kW of RF power per cavity.

2 SRF SYSTEM FOR CESR LUMINOSITY UPGRADE

2.1 SRF System Description

The superconducting RF system [6] consists of two RF stations (East and West). Each station includes two high-power klystrons, two single-cell superconducting niobium cavities in their individual cryostats (termed cryomodules), and a station cryogen distribution valve box (VB). In addition, a processing area (PA) can accommodate one cryomodule or a RF window assembly for high power testing and conditioning. Two klystrons in the East are 600 kW tubes manufactured by Philips. WR1800 waveguide can be arranged to feed two cavities (E1 and E2) from one klystron via magic T RF power splitter or to feed each cavity from its own klystron. In the West one klystron is also the 600 kW Philips tube, the other on is our newly acquired 800 kW tube manufactured by CPI. The first klystron is connected to the PA and used for various high power RF tests. The

CPI klystron provides RF power to two cryomodules (W1 and W2) located in the CESR West flare.

Liquid helium is provided by two 600 W refrigerators supplying 2000 liter storage dewar. Rigid transfer lines transport liquid helium, cold gaseous He, and liquid nitrogen between the refrigerator and storage dewar to a centrally located main distribution valve box. From the main valve box, rigid transfer lines lead to satellite valve boxes or directly to the superconducting elements supplying: 1) a pair of SRF cryomodules in the East RF station via a station VB; 2) a pair of SRF cryomodules in the West RF station via a station VB; 3) a SRF module in the PA via processing area VB; 4) the CLEO detector superconducting solenoid; 5) a pair of superconducting quadrupole magnets to be installed in the CESR IR as a part of the Phase III upgrade.

The rigid transfer lines have a heat leak of <0.5 W/m, contributing about 12 W per cavity feed. The largest heat leak is in the valves and flexible lines, contributing about 50 W per cavity feed. Thus, delivering liquid helium to four cryomodules consumes about 250 W of refrigeration power, which does not include the cryomodule heat load.
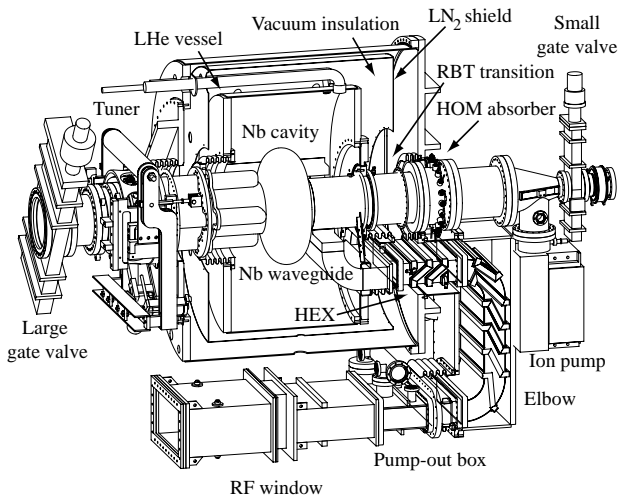

Figure 1. Layout of the B-cell cryomodule.

2.2 B-cell Cryomodule Layout, Preparation, and Tests

Some parameters of the Cornell B-cell cryomodule [7] are listed in Table 1, the cryomodule layout is shown in Figure 1. The 500 MHz single-cell niobium cavity resides inside a liquid helium vessel. The helium vessel is suspended inside the cryostat vacuum vessel by four ½ inch diameter Invar rods. The space between the helium vessel and the vacuum vessel walls serves as vacuum insulation. It also contains a thermal radiation shield maintained at liquid nitrogen temperature, two layers of magnetic field shielding, and layers of superinsulation.

The bell-shaped cavity has a big, 24 cm diameter, aperture. The big aperture beam pipes and "flutes" on one of them allow HOMs to escape the cavity. There are three main structural/thermal transitions between the cavity and external environment: a "fluted" beam tube (FBT), a round beam tube (RBT), and the rectangular waveguide RF feed. Ferrite-lined room temperature HOM loads are outboard of each beam pipe thermal transition. The FBT HOM load has a ring around which the cavity tuner clamps. The tuner mechanically adjusts cavity frequency via longitudinal elastic deformation allowed by bellows between the beam pipe and cryostat, with a large sliding joint outboard of the HOM load. The cavity round pipe is anchored to both helium and vacuum vessels.

Table 1: Parameters of the B-cell cryomodule.

Frequency	499.765 MHz
Accelerating field	6 - 10 MV/m
Effective cell length	0.3 m
Total RF voltage per cavity	1.8 - 3 MV
Cryomodule length	2.86 m
R/Q ($R=V^2/P$)	89 ohm
Q_0 at operating field (4.5 K)	$>10^9$
Q_{ext} of RF coupler	2×10^5
Cryostat static heat losses	30 W
Cryostat liquid He volume	520 liters
Loss factor of a module with one taper at $\sigma_z = 13$ mm	0.48 V/pC
HOM power at 1 A beam current	13.7 kW
RF power delivered to 1 A beam	325 kW
Number of cavities in CESR	4

Following the large sliding joint is a large 24 cm aperture inter-cavity gate valve, which maintains big aperture between two cryomodules. This reduces the cryomodule impedance since a significant portion of it is contributed by the tapers to CESR beam pipe [8, 9, 10].

The rectangular waveguide section immediately exterior to the helium vessel (HEX) is cooled by cold helium gas flowing through the tracing welded to the waveguide walls. Next is a waveguide double E-bend elbow similarly cooled by liquid nitrogen. Following this is a short thermal transition to room temperature, a waveguide vacuum pumping section, and finally the waveguide vacuum RF window. This waveguide path was dictated by tight space considerations in the CESR tunnel.

Prior to assembly, all major cryomodule components are subjected to acceptance tests. The cavity must achieve accelerating gradient greater than 6 MV/m with $Q_0>10^9$ in a vertical test [11]. All five our cavities passed acceptance test. In different tests five cavities reached

maximum accelerating gradients of 12 MV/m, 11 MV/m, 10 MV/m, 10 MV/m and 7.8 MV/m. The cavity with accelerating gradient of 7.8 MV/m has a thermal breakdown due to niobium material defect. The RF window must transmit more than 400 kW CW at 500 MHz traveling wave and experience >125 kW CW standing wave with the electric field maximum at the window ceramics [12]. Five out of six RF windows passed the test. One window failed due to ceramic heating caused by excessively thick titanium anti-multipacting coating. The assembled He and vacuum vessels with a dummy copper cavity insert must remain vacuum tight and demonstrate mechanical integrity upon cooling to liquid nitrogen temperature. The beam line HOM load consists of modular panels containing the RF absorbing element (ferrite) [13, 14]. The panels are individually prepared and tested to an average power density of 15.5 W/cm^2.

The cavity preparation procedure includes chemical etching by 1:1:2 buffer chemical polish (BCP) acid mix at the acid temperature below 15°C (to avoid cavity Q disease), high pressure rinsing and drying in a class 10 clean room where the niobium cavity insert is assembled afterwards. All high vacuum components are vacuum baked. After assembly is complete, a cryomodule must pass a final high power acceptance test in the PA. It must demonstrate ability to deliver accelerating gradient of >6 MV/m and have static heat leak of ≈30 W. All four cryomodules installed in CESR to date have passed this test. The fifth, spare, cryomodule is being assembled.

2.3 Controls, Data Acquisition and Diagnostic Tools.

A cryomodule is equipped with a set of sensors to monitor temperature at different points, cavity and insulation vacuum, helium bath pressure, and cooling water flow. For cryogenic temperature measurements we use Cryogenic Linear Temperature Sensors (CLTS) [15] and carbon thermometers. A cryogenic venturi-type flow meter was developed to measure the cold gas mass flow in the helium return line [16]. The helium mass flow measurements are used to calculate cryomodule heat load both with and without RF.

Each cryostat has five cryogenic feedback loops. The station cryogen distribution box contains the supply and return pneumatic valves to regulate liquid helium level and helium bath pressure inside the He vessel correspondingly. The helium level is kept constant within ±1%, and the pressure is kept constant within ±0.02 psi. Another feedback loop keeps waveguide HEX gas flow constant by regulating a gas flow valve installed in the HEX return line. Last two loops control helium and nitrogen gas temperatures in the warm return lines. A key control for stable refrigerator operation was found to be maintaining a steady cold helium gas flow

rate from the various heat loads. Since SRF cavity heat deposition varies with RF field level, an analog electronic circuit was implemented to heat a resistive load in the cryostat He vessel at the difference between a chosen "level load" and the dynamic RF load. The level is nominally set at 60 W.

Cryomodules have several layers of protection against excessive He bath pressure, which can damage the cavity. If the He bath pressure reaches 10 psi, the safety valve opens releasing pressure and sending helium gas via the vent line outside the CESR tunnel. If safety valve fails to lower cryostat pressure and pressure reaches 15 psi, then burst disk will rupture and let helium gas go to the vent line. The cause of excessive pressure could be, for example, a refrigerator trip or malfunctioning, or a cavity quench. In case of refrigerator trip/malfunctioning pressure in the warm helium gas return line becomes high. A circuit watching his pressure will close all valves connecting He vessel to the refrigeration system and turn off power to the He vessel resistive load, isolating cryomodule and letting safety valve to protect the cryostat. In case of cavity quench it is imperative to turn off RF power to the cavity as rapid as possible to prevent cavity damage due to overheating. The first and fastest layer of protection is a quench detector described below. If it fails to shut RF down, then there is a fast mechanical pressure switch set to 7.5 psi, which will trip RF power.

The quench detector has the same two modes of operation as the rest of RF system: processing mode and run mode. In the processing mode a RF feedback loop regulate power reflected from the cavity. Since RF coupler has very strong coupling to the cavity without beam loading, almost all incident RF power is reflected back to klystron. When superconducting cavity is in transition to normal conducting state, coupling is going toward optimal, i.e. reflected power is going down. Therefore the quench detector shuts RF down as soon as reflected power is below the set point (certain percentage of forward power). In the run mode feedback loop regulates amplitude of cavity RF field. Reflected power is going down naturally with increasing beam loading. Hence, apart from detecting low level of reflected power, quench detector circuit watches RF field amplitude as well. RF shutdown signal is generated only if both reflected power and cavity field are below corresponding set points. Also, in both modes it is possible to set trip level for a maximum forward power.

There is an interlocks ready chain for each cryomodule, which must be set before one can turn RF power on. It includes various alarm signals, such as liquid helium level, helium bath pressure, HEX gas flow, miscellaneous temperatures and cooling water flows, cavity vacuum, cryostat insulation vacuum, cavity tuner position and force, RF window arc detector, quench detector, CESR tunnel secure, etc. Any one of these signals can trip RF system. Some of them are latched,

some are non-latched, depending on the severity of the problem and on the system ability to recover by itself. All RF-related trips are non-latched (quench detector, window arc, window vacuum).

All SRF signals are connected to the CESR data acquisition system. In addition to this, a new graphics display system based on the GDL language [17] is used to display data in real time on a X-terminal. The GDL system provides such features as labeled schematics, strip charts, meters, and tables.

The SRF system has all standard features of an accelerator RF system: amplitude feedback loop, tuning angle loop, RF phase loop, etc. As it was mentioned above, two cavities are fed from one klystron via magic T. CESR RF system uses so-called "master–slave" configuration for the cavity field regulation, when a cavity field signal from only one cavity is used in the feedback loop. The other cavity passively follows by virtue of the cavities similarity. It becomes more complicated when one has two different cavities in a pair as we had after installation of our first SRF cavity in the ring. To maintain the same RF field as the copper cavity, the SRF cavity requires much less incident power without beam present. For example, to get accelerating voltage of 1.5 MV, one needs to provide forward power of approximately 100 kW to the NRF cavity, but only about 30 kW to the SRF cavity with nearly all of it reflected. The numbers converge with increasing beam current, but even at 0.6 A total beam current we get forward power of 250 kW for the NRF cavity versus 210 kW for the SRF cavity. In order to keep voltages reasonably even, it was proposed to use a waveguide 4 dB hybrid instead of magic T as an RF power splitter [18]. In the 4 dB splitter configuration the SRF cavity was operated at a field of 6.3 MV/m or voltage of 1.9 MV while NRF cavity accelerating voltage varied with beam current. With two SRF cavities in a pair, "master" is always the weaker cavity, i.e. the cavity with lower accelerating field limit. RF phase loop regulates the sum of RF phases of two cavities in a pair.

RF system signals (forward and reflected power, cavity field, cavity phase and tuning angle) for each cavity are incorporated in the CESR beamloss diagnostic system [19]. The system is a turn-by-turn data acquisition system based on COMET™ VME multichannel analog digitizer boards. This allows us to analyze beamloss events in which the RF system trips to determine if beam motion contributed to the trip, or if the beam was stable at the point of trip. RF system can trip due to different causes: cavity quench, arcing or multipacting in the vacuum waveguide or at the ceramic RF window, regulation problems, cryogenic system problems, etc. Fortunately, different trip events have different "signature" of RF signal envelopes that makes it somewhat easier to distinguish different problems (see example in Figure 2).
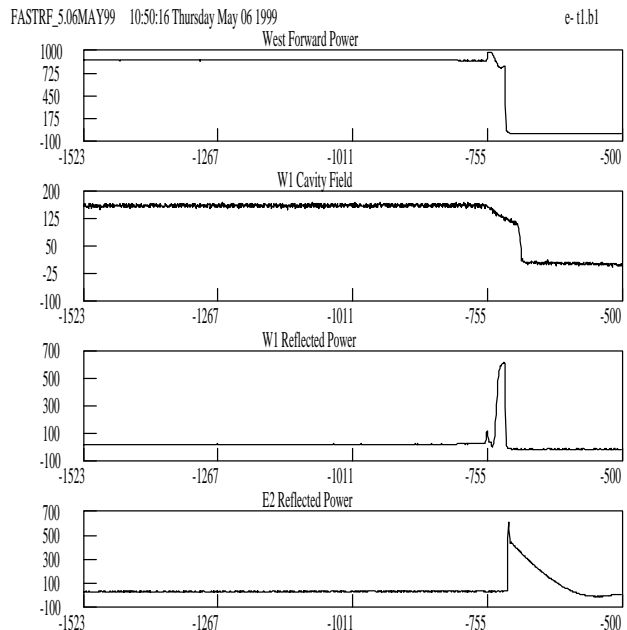

Figure 2. W1 cavity waveguide arc event. Shown are the forward power, cavity field and reflected power for the W1 cavity and reflected power for E2 cavity. The *x*-axis is sample number, where a sample is taken every 280 ns.

3 INSTALLATION AND COMMISSIONING RESULTS, OPERATING EXPERIENCE

The RF system replacement began in 1997 and was performed in stages, with installation of SRF cryomodules one at a time in place of old normal conducting cavities.

The first SRF cavity (E2) was installed in CESR in September 1997. During the commissioning phase, CESR beam currents were limited by travelling wave power (forward power – reflected power) which could be tolerated by the cavity input coupler. We observed high vacuum trips at rather repeatable power levels due to gas evolution brought on by multipacting in the window and coupler region. Two processing techniques have proven useful in raising the travelling wave power limits. The greatest success so far has been achieved when processing without beam by increasing power in the pulsed mode on or close to cavity resonance. Such processing allows us to process the coupler region in the travelling wave mode. Because the SRF cavity is heavily overcoupled without beam, the emitted power at RF shut-off is four times higher than the incident power. This creates the travelling wave mode for a very short time though. Changing the frequency around resonance shifts the standing wave pattern in the waveguide, and

processes its different regions. Above 90-100 kW forward power, the cavity quenches and becomes close to matched load. At this and higher powers we disable the quench detector and allow the cavity to sit in quench state for entire duration of pulse, typically 10 ms at 10% duty cycle. We found that after pulse processing the travelling wave power limit with beam could be raised from 100 kW to 140 kW. At this power level we observed for a first time dependence of the RF power on the cavity field: transmitted power is higher when there is bigger standing wave component. Computer simulations [20] confirmed that travelling to standing wave mixing ratio affects multipacting bands.

Another processing technique that has been useful is to process with stored beam and continue to raise the travelling wave power by adjusting the relative phase between two RF stations. A software program has been developed to automatically adjust the relative phase while monitoring RF vacuum signals.

A second variety of vacuum trips arose from RF heating of the waveguide thermal transition section. Such vacuum events showed a measurable temperature rise on the transition section, and were accompanied by a large release of hydrogen as observed on an RGA. Presumably cryosorbed hydrogen was released as the surface was heated. Analysis of the residual gas evolution [21] during cavity warm up showed that during 3 months of operation cold surfaces accumulated up to 7 equivalent monolayers of hydrogen. RGA spectra showed different gas species. Most pronounced among them are hydrogen, carbon monoxide, and water vapour.

After warming up the cavity to room temperature and baking the window *in situ* to 110°C during scheduled CESR shutdown, the beam power delivered began to rise steadily and reached 180 kW. After about 2 months in operation, the ability of the cavity to deliver RF power began to deteriorate again due to the fast vacuum trips. After another warmup the E2 power delivered to beam eventually reached 212 kW. Experience with the first SRF cavity suggested modification to the cryomodule design and handling procedures, which were incorporated into subsequent installations [22].

When the second (E1) cryomodule was tested at high power in the processing area, the cavity quenched at gradient around 5 MV/m, below the 6 MV/m acceptance threshold and significantly below 11 MV/m reached in a vertical test. A CLTS thermometer on the equator bottom showed a 50 K temperature rise during quench, indicating contaminant found its way into the cavity. Since disassembly and re-assembly of the cryomodule to re-etch the cavity is a several month long procedure, we performed a risky operation of using a long stick to wipe the cavity equator bottom in situ [22]. Several small particles were removed from the cavity. The largest of them had size of approximately 100 μm (Figure 3). X-ray analysis showed the spherical object to be nearly pure Fe and the attached flake to contain Fe, Cr, and Ni,

indicating partially melted stainless steel. Apparently, a stainless sliver from a sheared tongue and groove seal migrated to the cavity bottom and partially melted during high power RF testing. Fortunately, the melted stainless steel did not wet well to the niobium, and after removal, cavity performance improved considerably, exceeding the 6 MV/m acceptance threshold. The same thermometer indicates that quenches at the high gradient still originate at the cavity equator bottom. The second cavity was installed in October 1998 and reached 218 kW within one month of operation.
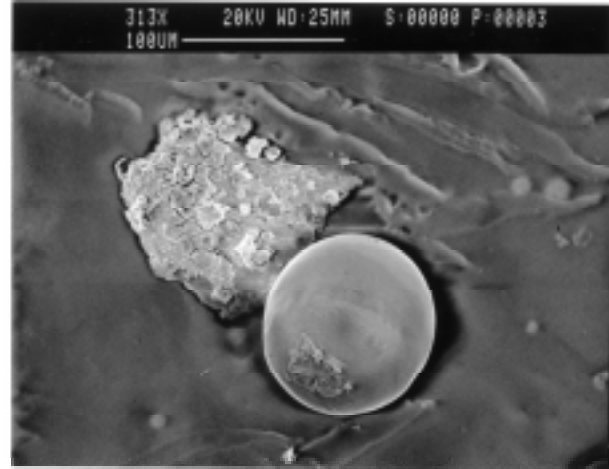

Figure 3. SEM photo of a partially melted stainless steel sliver wiped from the equator bottom of the E1 cavity.

The third (W1) cavity was installed in March 1999. A short 6-week running period in April-May 1999 was devoted to commissioning the new SRF cavity, exploring beam current limits and running beams for CHESS experimental users. At first, the vacuum waveguide arcs discussed above limited the power, delivered to the beam by this cavity. The cavity was warmed up to 50 K to remove absorbed hydrogen. Following this warm up and subsequent high-power pulsed processing the beam power delivered through W1 increased from 140 kW to 260 kW. The power delivered to the beam by each of three superconducting cavities is shown in Figure 3. Typically, the SRF cavities have operated in the range of 5-7 MV/m. The last cavity (W2) was installed in September 1999 and awaits commissioning in November 1999.

Since early 1996 CESR beam currents have begun to be limited by a longitudinal coupled bunch instability due to high Q factor of parasitic modes in normal conducting RF cavities [23]. A staged replacement of the normal conducting RF allowed us to study the impact on longitudinal threshold instability at each step [24, 3]. The instability threshold increases with SRF cavities installation are not quite as dramatic as we might have expected. A detailed calculation and comparison to

threshold data has been performed. The analysis showed good agreement between calculations and measurements for the case of four normal conducting RF (NRF) cavities and three NRF plus one SRF, but began to worsen for the two NRF plus two SRF case. These results suggest that as NRF cavities are removed, the impedance of the rest of the ring becomes more important and dominates the longitudinal dynamics when all NRF cavities are removed.
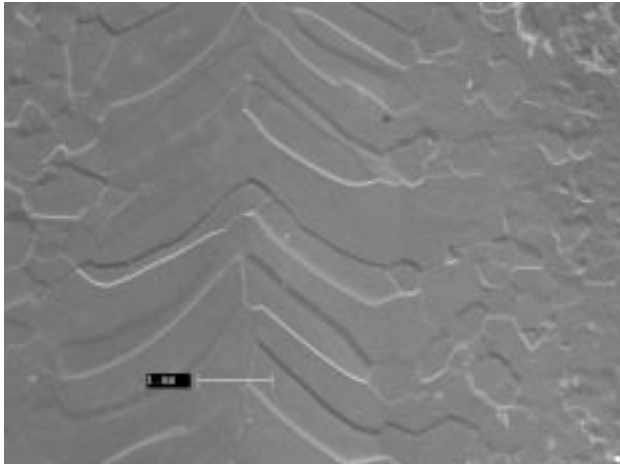
(a)
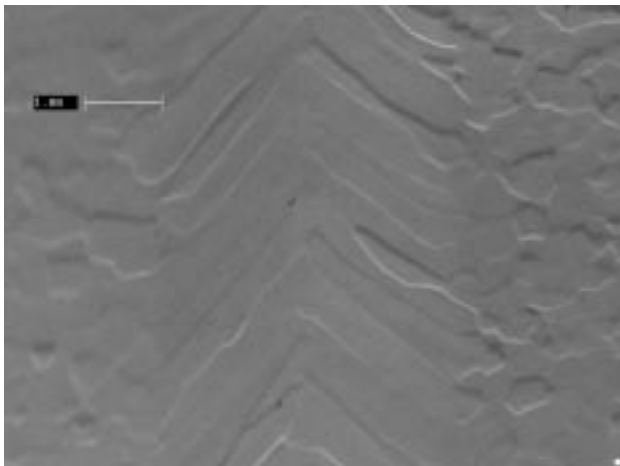
(b)

Figure 4. The surface of EBW region of the niobium sample after a surface removal of 117 μm by BCP (a), and after an extra removal of 90 μm by EP (b).

4 BASIC SRF STUDIES

Quality factor slope in field-emission-free cavities at high accelerating gradients (>20 MV/m) has been observed at a number of laboratories. A model, based on magnetic field enhancement at grain boundaries, was developed at Cornell and used to simulate the measured Q-slope results [25]. It can account for differences in cavity behaviour following 140°C and 850°C heat treatment. The model also explains a number of other observations, such as improved cavity performance following electrolytic polishing (EP), as well as the predominant quenches at the equator weld in chemically etched cavities.

The study of the micro-structure of RF surfaces in the electron beam weld (EBW) region of niobium produced some interesting results [26]. The EBW surfaces were polished with different techniques, namely 1:1:2 BCP and with EP. It was found that grain boundaries near the center line of the EBW are nicely lined up almost perpendicular to the center line. Upon polishing with BCP, these grain boundaries evolve into micro-steps with sharp edges. In contrast, EP reduces dimensions and rounded off sharp edges of surface irregularities (see Figure 4). These observations have important implications in explanation of the Q-slope.

The mushroom cavity proved to be a very useful tool in studying effects of strong electromagnetic fields on metal surfaces in the past [27]. Recently we decide to revive this tool. Some improvements in new design include stronger fields concentrated over a smaller region, higher Q factor, and more robust construction [28].

5 SUMMARY AND FUTURE PLANS

Cornell design of a superconducting HOM-damped cavity cryomodule for high-current electron storage ring proved to be successful. Staged installation of SRF cavities in CESR helped to increase total beam current to 550 mA and peak luminosity to 8.3×10^{32} cm^{-2}s^{-1}. With installation of the final cavity in September 1999 we will be able to increase CESR beam current an luminosity further and ultimately reach its Phase III luminosity goal.

Based on the successful operating experience with SRF cavities in CESR and KEK-B, several light sources are considering the adoption of SRF cavity solution for their rings [29, 30].

We continue R&D efforts to develop an HOM-damped cryomodule of the next generation for the new two-in-one collider with the luminosity goal of 3×10^{34} cm^{-2}s^{-1} [31, 32]. In particularly, significant efforts are devoted to high average RF power window and coupler development [33].

6 REFERENCES

[1] S. Belomestnykh, "The High Luminosity Performance of CESR with the New Generation Superconducting Cavity," *Proc. of the 1999 Part. Accel. Conf.,* Vol. 1, pp.272-276.

[2] S. Belomestnykh, et al., "Commissioning of the Superconducting RF Cavities for the CESR Luminosity Upgrade," *Proc. of the 1999 Part. Accel. Conf.,* Vol. 2, pp.980-982.

[3] S. Hensderson, "CESR Performance and Upgrade Status," presented at the e+e- Factories 1999 (to be published), also, Cornell LNS Report CBN 99-28.

[4] S. B. Peck, D. L. Rubin, "CESR Performance and Upgrade Status," *Proc. of the 1999 Part. Accel. Conf.,* Vol. 1, pp.285-287.

[5] H. Padamsee, et al., "Design Challenges for High Current Storage Rings," *Part. Accel.,* **40**, pp. 17-41 (1992).

[6] S. Belomestnykh, et al., "Superconducting RF System for the CESR Luminosity Upgrade: Design, Status, and Plans," *Proc. of the 5th European Part. Accel. Conf.,* Vol. 3, pp. 2100-2103.

[7] J. Kirchgessner, et al., "Superconducting RF Activities at Cornell University," *Proc. of the 7th Workshop on RF Superconductivity,* Vol. 1, pp. 35-37.

[8] V. Veshcherevich et al., "The Loss Factor of the Cavity Module for the CESR Beam Test and Some Other Asymmetric Structures," Cornell LNS Report SRF 931013-11 (1993).

[9] S. Belomestnykh and W. Hartung, "Calculations of the Loss Factor of the BB1 Superconducting Cavity Assemblies," Cornell LNS Report SRF 960202-01 (1996).

[10] S. Belomestnykh, "On the BB1 Cryomodule Loss Factor Calculations," Cornell LNS Report SRF 990714-08 (1999).

[11] D. Moffat, et al., "Preparation and Testing of a Superconducting Cavity for CESR-B," *Proc. of the 1993 Part. Accel. Conf.,* Vol. 2, pp. 763-765.

[12] E. Chojnacki, et al., "Tests and Designs of High-Power Waveguide Vacuum Windows at Cornell," *Part. Accel.,* **61**, pp. [309-319]/45-55 (1998).

[13] S. Belomestnykh, et al., "Comparison of the Predicted and Measured Loss Factor of the Superconducting Cavity Assembly for the CESR Upgrade," *Proc. of the 1995 Part. Accel. Conf.,* Vol. 5, pp. 3394-3396.

[14] E. Chojnacki, W. J. Alton, "Beam Line RF Load Development at Cornell," *Proc. of the 1999 Part. Accel. Conf.,* Vol. 2, pp.845-847.

[15] Micro-Measurements Division, Measurements Group, Inc.

[16] M. Forster and J. Graber, "Cryogenic Venturi-type Flow Meters," SRF Internal note, 1996.

[17] R. Geng and S. Peck, "Graphics Display of CESR SRF Parameters," Cornell LNS Report SRF/D 980407-01 (1998).

[18] S. Belomestnykh, et al., "Beam Installation of the BB1-2 Cavity: Waveguide Adjustment and Cavity Positioning," Cornell LNS Report SRF961217-04.

[19] S. Henderson, "A Beamloss Diagnostic System for CESR," *Proc. of the 1997 Part. Accel. Conf.,* Vol. 2, pp. 2029-2031.

[20] R. L. Geng and H. Padamsee, "Exploring Multipacting Characteristics of a Rectangular Waveguide," *Proc. of the 1999 Part. Accel. Conf.,* Vol. 1, pp.429-431.

[21] R. L. Geng and H. Padamsee, "Absorption and Evacuation of Residual Gases in the SRF System for the CESR Luminosity Upgrade," *Proc. of the 1999 Part. Accel. Conf.,* Vol. 2, pp.983-985.

[22] E. Chojnacki and J. Sears, "Superconducting RF Cavities and Cryogenics for the CESR III Upgrade," presented at the 1999 Cryogenic Engineering and Intl. Cryogenic Materials Conf. (to be published), also, Cornell LNS Report SRF990716-09.

[23] M. Billing, "Observation of a Longitudinal Coupled Bunch Instability with Trains of Bunches in CESR," *Proc. of the 1997 Part. Accel. Conf.,* Vol. 2, pp. 2317-2319.

[24] M. G. Billing and S. Belomestnykh, "Observations of a Longitudinal Coupled Bunch Instability in CESR," *Proc. of the 1999 Part. Accel. Conf.,* Vol. 2, pp.1112-1114.

[25] J. Knobloch, et al., "High-Field Q Slope in Superconducting Cavities Due to Magnetic Field Enhancement," *this proceedings.*

[26] R. Geng, et al., "Micro-Structures of RF Surfaces in the Electron Beam Weld Region of Niobium," *this proceedings.*

[27] D. Moffat, et al., "Studies of the Nature of Field Emission Sites," *Part. Accel.*, **40**, pp. 85-126 (1992).

[28] G. Werner, et al., "The Mushroom Cavity for the Next Millennium," *this proceedings.*

[29] R. C. Sah, et al., "Status of the Taiwan Light Source," *Proc. of the 1999 Pat. Accel. Conf.,* Vol. 4, pp. 2415-2416.

[30] H. Padamsee, "The Future of SRF in High Current Rings," *this proceedings.*

[31] A. Mikhailichenko and D. Rubin, "Concentric Ring Colliding Beam Machine with Dual Aperture Quadrupoles," *Proc. of the 5th European Part. Accel. Conf.,* Vol. 1, pp. 433-435.

[32] D. Rubin, et al., "Dual Aperture High Luminosity Collider at Cornell," *Proc. of the 1997 Part. Accel. Conf.,* Vol. 1, pp. 318-320.

[33] E. Chojnacki and S. Belomestnykh, "RF Power Performance at CESR and Designs of Multipactor Inhibited Couplers," *this proceedings.*